Article

Journal of
Nanoscience and Nanotechnology
Vol. 21, 1483–1492, 2021
www.aspbs.com/jnn

Fabrication of Mesoporous C_{60}/Carbon Hybrids with 3D Porous Structure for Energy Storage Applications

Arun V. Baskar[1], Jefrin M. Davidraj[1], Ajanya M. Ruban[1], Stalin Joseph[1], Gurwinder Singh[1], Ala'a H. Al-Muhtaseb[2], Jang Mee Lee[1], Jiabao Yi[1], and A. Vinu[1,*]

[1] *Global Innovative Center for Advanced Nanomaterials, The University of Newcastle, Callaghan, New South Wales 2308, Australia*
[2] *Department of Petroleum and Chemical Engineering, College of Engineering, Sultan Qaboos University, Muscat 123, P.O. Box 33, Oman*

We report on the synthesis of 3D mesoporous fullerene/carbon hybrid materials with ordered porous structure and high surface area by mixing the solution of fullerene and sucrose molecules in the nanochannels of 3D mesoporous silica, KIT-6 via nanotemplating approach. The addition of sucrose molecules in the synthesis offers a thin layer of carbon between the fullerene molecules which enhances not only the specific surface area and the specific pore volume but also the conductivity of the hybrid materials. The prepared hybrids exhibit 3D mesoporous structure and show a much higher specific surface area than that of the pure mesoporous fullerene. The hybrids materials are used as the electrodes for supercapacitor and Li-ion battery applications. The optimised hybrid sample shows an excellent rate capability and a high specific capacitance of 254 F/g at the current density of 0.5 A/g, which is much higher than that of the pure mesoporous fullerene, mesoporous carbon, activated carbon and multiwalled carbon nanotubes. When used as the electrode for Li-ion battery, the sample delivers the largest specific capacity of 1067 mAh/g upon 50 cycles at the current density of 0.1 A/g with stability. These results reveal that the addition of carbon in the mesoporous fullerene with 3D structure makes a significant impact on the electrochemical properties of the hybrid samples, demonstrating their potential for applications in Li-ion battery and supercapacitor devices.

Keywords: Mesoporous, Fullerene, Energy Storage, Li-Ion Battery, Supercapacitor.

1. INTRODUCTION

The ever increasing demand for the clean energy in the current century has triggered the researchers to put significant efforts on the design and the development of clean energy storage and conversion based devices [1–4]. Among these devices, the supercapacitors and batteries are leading the commercial market due to their high power density and energy density [5–8]. The performance of these devices is mainly linked with the types of electrode materials used in the devices and their properties. Therefore, much attention has been given on the design and the development of novel and advanced electrode materials with high specific surface area, high electronic conductivity and low cost. Various electrodes materials, including carbons, nitrides, fullerenes, oxides, and metals, have been used as electrodes for these applications [9–11]. Among these electrodes, carbon-based electrodes have been receiving a lot of attention for these devices owing to their low cost and electrochemical properties. For example, activated carbon, CNT and graphene hold great importance in both supercapacitor and lithium-ion battery [12–18]. Although these materials were found to be interesting for these applications, the performance of the devices based on these materials can be improved by hybridising with different nanostructures. Recently, the development of electrode by mixing and hybridising two or more carbon nanostructures has gained paramount importance [19–23]. For instance, 3D graphene/CNT was developed by CVD technique and showed improved specific capacitance (197.2 F/g) over pure 3D graphene (36.5 F/g) [24]. It was shown that the incorporation of CNT between the graphene layers provides an enhanced electrical conductivity and further prevents the aggregation of graphene, resulting in improved performance. In another report, the selection of optimum graphene/CNT ratio was found to alter the specific capacity of the lithium-ion battery showing a maximum capacity of 303 $mAhg^{-1}$ for 70 wt% graphene [25]. Although there are a lot of reports on mixed carbon-based

*Author to whom correspondence should be addressed.

electrodes, the development of novel low-cost precursors using facile synthesis methods to give highly ordered structure is still challenging.

Among the allotropes of carbon, fullerene is quite unique owing to its structure and electronic properties. The properties of the fullerenes can be easily altered through hybridisation with different nanostructures and functionalisation [26–32]. Among the different properties, its electron accepting nature is one of the highlights and makes it a promising material for energy storage and conversion. For example, hydrogenated C_{60} was used for the lithium-ion battery as an anode material with good stability and capacity of 588 mAh/g [33]. Very recently, Vinu and his co-workers introduced ordered mesoporosity in the fullerene nanostructures with different carbon atoms through nanotemplating approach using mesoporous silica as templates and employed them as electrodes for supercapacitor applications [34–35]. Although these mesoporous fullerene nanostructures showed interesting energy storage properties, its cost makes a major hurdle in commercialising the technology. The properties and the performance of these materials in energy application could be enhanced by hybridising with metal oxide nanostructures, including iron oxide or copper oxides [36–37]. However, the preparation steps involve multiple steps which makes the whole process expensive. To overcome these challenges, the mixing of other cheap and conducting carbon precursors can be favourable. In this paper, fullerene is used as the precursor alongside with sucrose and polymerised in the nanochannels of mesoporous silica with 3D porous structure which is used as a template. Unlike our previous work [36–37], here, we used KIT-6 as a 3D sacrificial nano template. We demonstrate that by integrating two-step polymerisation of the carbon precursors and hard templating strategy, novel mesoporous fullerene/carbon hybrids with 3D structures and enhanced textural properties can be obtained. By integrating with low-cost carbon precursor, the cost of the whole process can be reduced for the fabrication of the materials without sacrificing the electrochemical and textural properties.

Further, the 3D cubic structure of the hybrid provides better structural stability and ion mobility compared to mesoporous carbon from 2D SBA-15 template. These hybrids materials have also been used as electrodes for supercapacitor and Li-ion battery applications. The prepared hybrids show much better performance than other carbon-based porous materials, further demonstrating their potential for advanced energy storage and conversion devices.

2. EXPERIMENTAL DETAILS

2.1. Materials and Reagents

The pluronic surfactant P123 ($EO_{20}PO_{70}EO_{20}$, molecular mass = 5750), silica precursor tetraethyl orthosilicate (TEOS), organic solvent 1-chloronapthalene for dissolving

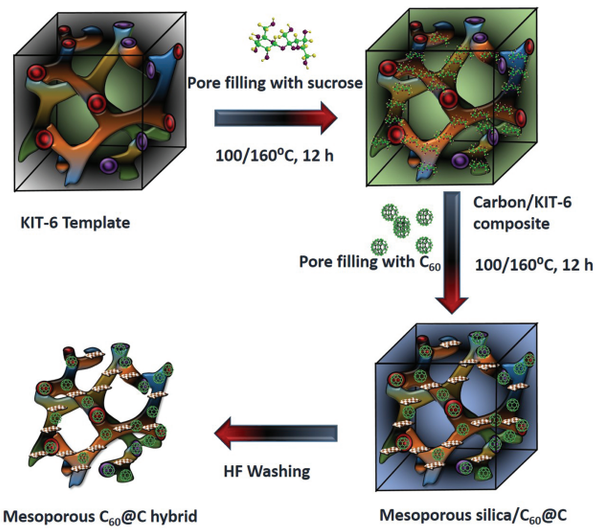

Scheme 1. Schematic representation of MC_{60}@C-X-K hybrids prepared by using KIT-6 as a template through nanohard templating approach.

C_{60}, pH maintaining acid HCl and H_2SO_4 are obtained from Sigma Aldrich. High purity C_{60} (99.5%) is obtained from Solaris Chem. All the materials are used as received without further purification.

2.2. Synthesis of 3D Mesoporous Carbon/C_{60}

To make our desired material mesoporous carbon/mesoporous fullerene hybrids (Scheme 1), sucrose and fullerene in 1-chloronaphthalene were infiltrated into the nanochannels of KIT-6-150 template. In this work, we have used KIT-6 material prepared at 150 °C. The detailed procedure for the synthesis of KIT-6-150 can be found elsewhere [38]. For making mesoporous carbon/mesoporous fullerene hybrids, the calculated amount (100 mg, 150 mg, 200 mg and 250 mg) of sucrose in 5ml of water and 50 μl of H_2SO_4 was added to 1g of KIT-6-150 prepared at 150 °C. Then, the mixture was kept in a hot oven for 6 hours at 100 °C and 6 hours at 160 °C. Subsequently, the resultant mixture was pore filled with a sonicated solution of 5 g 1-chloronapthalene and 200 mg C_{60}. This carbon/C_{60}/KIT-6 composite was kept in a tubular furnace at 900 °C for 5 hours. The final product was treated with 5 wt% HF to remove the mesoporous silica template. The samples are denoted as MC_{60}-@C-X-K, where X denotes the weight ratio of C_{60} and sucrose.

3. RESULTS AND DISCUSSION

The structural order of the prepared MC_{60}@C-X-K hybrids was investigated by powder X-ray diffraction measurements, and the results are shown in Figure 1. Figure 1(A) shows the low angle powder X-ray diffraction patterns of

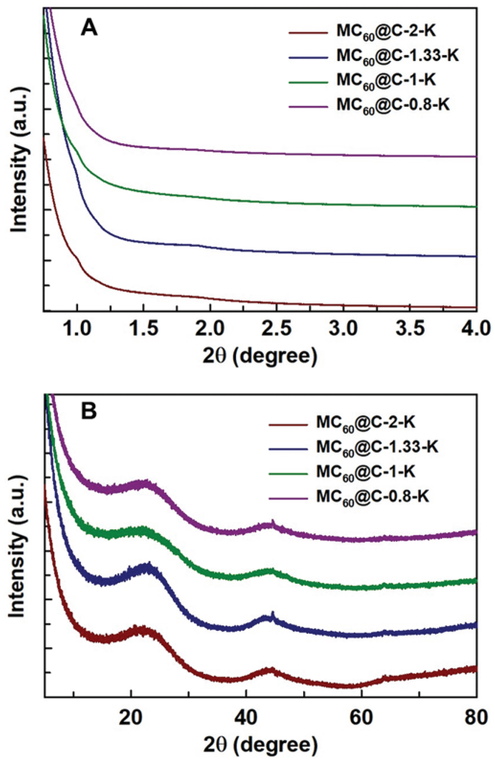

Figure 1. (A) Low angle and (B) wide angle powder X-ray diffraction patterns of MC_{60}@C-X-K hybrids.

MC_{60}@C-X-K hybrids prepared at different sucrose contents using KIT-6-150 as the template. All the samples showed a peak at a lower angle, demonstrating the presence of mesoporous structure in the samples. However, the samples did not show any higher-order peaks, revealing a slight disorder in the samples. Interestingly, the d-spacing of the samples was not much affected upon the addition of the sucrose molecules. This observation indicates that the addition of the sucrose molecules in the synthesis mixture does not make much influence on the unit cell constant of the hybrid samples. It should be noted that the lower angle peak of MC_{60}@C-0.8-K was a bit broader as compared to other indicating that the structural order of the sample was affected when the amount of the sucrose molecules in the synthesis mixture is high. The effect on the crystallinity of the carbon walls of the hybrid materials as well as the formation of polymerised fullerene was investigated by wide-angle powder X-ray diffraction, and the results are shown in Figure 1(B). The prepared hybrid samples showed two broad peaks centered ca 22.35 and 44.7°, which correspond to (002) and (100) planes and are indicative of turbostratic carbon wall structure. It should be noted that the intensity of these peaks gets more suppressed for MC_{60}@C-1.33-K as compared to other samples. The absence of the higher-order and sharp peaks related to the polymerised fullerene indicates that the polymerisation of the fullerene molecules was slightly affected by the addition of sucrose molecules as it is believed that the sucrose molecules form a thin layer of carbon between the fullerene molecules.

Table I. Textural parameters of MC_{60}@C-X-K hybrids.

Sample name	SA (cm^2/g)[b]	PD (nm)[c]	PV (cm^3/g)[d]
MC_{60}@C-2-K	791	2.6	1.1
MC_{60}@C-1.33-K	817	2.6	1.1
MC_{60}@C-1-K	988	2.6	1.3
MC_{60}@C-0.8-K	890	2.7	1.1

The surface properties, including specific surface area, pore volume and the pore diameter of the prepared hybrids were measured by nitrogen adsorption-desorption measurements, and the results are given in Table I and Figure 2. As can be seen in Figure 2(A), all the samples show type IV isotherm which is typical of mesoporous materials, revealing that the pores of the materials are not blocked after the introduction of additional carbon species through the addition of sucrose molecules. All the samples display a broad hysteresis loop at a higher relative pressure (>0.5 P/P_0), suggesting the presence of mesopores in the samples. However, the amount of nitrogen adsorbed at the monolayer region which is generally used for the calculation of the specific surface area of the materials increases with decreasing the weight ratio of C_{60}/S from 2 to 1 and then decreases at 0.8. The specific surface area increases

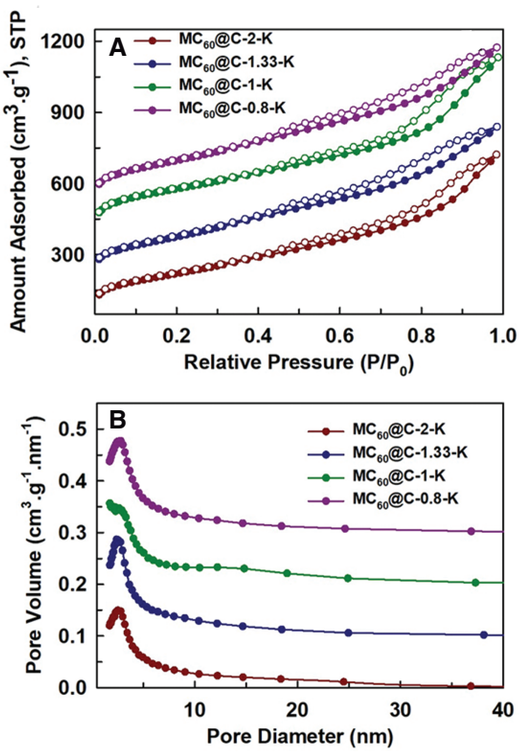

Figure 2. (A) Nitrogen adsorption–desorption isotherms and (B) BJH adsorption pore size distributions of MC_{60}@C-X-K hybrids.

from 791 to 988 m^2/g when the C_{60}/S ratio is decreased from 2 to 1 and then decreases to 890 m^2/g for MC_{60}@C-0.8-K. A similar trend is also observed for the pore volume of the samples, which increases from 1.1 to 1.3 cm^3/g and then decreases to 1.1 when the C_{60}/S ratio is decreased to 0.8. These results indicate that the addition of sucrose molecules plays a significant role in controlling the surface properties of the samples. This is mainly due to the fact that the sucrose molecules help to connect the fullerene molecules as well as create nanochannels during the carbonisation process. This is crucial for the energy storage and conversion application as it helps for the better transport of electrons and the electrolytes and is expected to enhance the charge transfer kinetics and further offer more electrochemically active sites. Among the samples prepared, MC_{60}@C-1-K exhibits the highest specific surface area and the specific pore volume. Figure 2(B) shows the BJH pore size distribution of MC_{60}@C-X-K hybrid samples. It can be seen that the pore diameter of the samples is in the range of 2.6 to 2.7 nm, suggesting that the addition of sucrose molecules does not make any influence on the size of the pores. However, all the samples show a broad condensation step at higher relative pressures which can be attributed to the presence of large voids in the samples. These voids are generated through the incomplete filling of the pores with either sucrose molecules or fullerenes in the pores of the templates. This creates large voids upon the removal of the template through HF treatment.

The Raman spectra of all the MC_{60}@C-X-K samples are shown in Figure 3. All the samples show two bands centered ca 1340 (D Band) and 1588 cm^{-1} (G Band), which are typically observed for the porous carbon samples. The peak at 1340 cm^{-1} (D band) is attributed to the defects and the disordered carbon wall structures whereas the peak at 1588 cm^{-1} is assigned to the sp^2-hybridised graphitic carbons in the wall structure. The amount of disorder and the defects in the carbon wall structure of the hybrids as the function of carbon from the sucrose was also measured from the intensity ratio of D and G bands (I_D/I_G). The value of I_D/I_G is higher for MC_{60}@C-2-K than that of MC_{60}@C-1.33-K and MC_{60}@C-1.33-K.

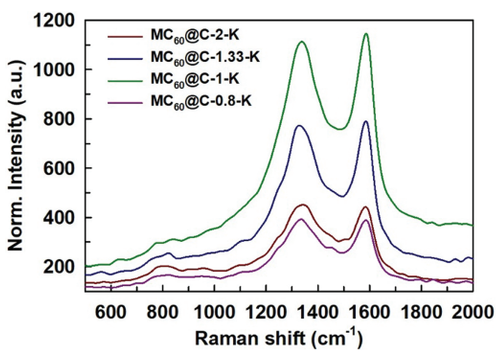

Figure 3. Raman spectra of MC_{60}@C-X-K hybrids.

Among the samples studied, MC_{60}@C-1-K registered the lowest I_D/I_G ratio, revealing better crystallinity in the sample. As expected, the I_D/I_G of MC_{60}@C-0.8-K is higher than that of MC_{60}@C-1.33-K and MC_{60}@C-1.33-K, which could be attributed to a large amount of the sucrose in the sample which forms carbon walls with large voids and a large number of defects.

The chemical composition and the bonding characteristics of carbon and the oxygen in the MC_{60}@C-X-K hybrids were analysed by X-ray photoelectron spectroscopy, and the results are shown in Figure 4. Figure 4(A) reveals the survey spectra of MC_{60}@C-X-K hybrids. As can be seen in Figure 4(A), the samples contain a large amount of carbon together with a small amount of oxygen which is originated from the sucrose molecules. The total amount of oxygen in the MC_{60}@C-2-K is much higher than that of other samples in this study, suggesting that the oxygen molecules mainly come from the sucrose molecules as well as the incomplete reaction between the fullerene molecules and the sucrose molecules for MC_{60}@C-2-K. Figures 4(B)–(E) shows the C1*s* spectra of all the samples, which could be deconvoluted into four peaks at 284.4, 285.5, 286.9, and 289.2 eV (Figs. 4(B–E)). The peak at the lowest binding energy is assigned to the sp^2-hybridised graphitic carbon atoms which is originated from either the fullerene molecules or the graphite from the sucrose molecules. The highest binding energy peak can be assigned to the strong π–π^* interaction between the partially graphitic carbon layers of the hybrid samples. On the other hand, the peaks at 285.5 eV and 286.9 are assigned to –C–OH/–C–O and –C═O groups, respectively. These peaks are originated from the incomplete conversion of the sucrose molecules into graphitic carbons or the partial oxidation of fullerene molecules from the oxygen from the sucrose molecules. The O1*s* spectra of the hybrid samples are shown in Figures 4(F)–(I), and the peaks could be deconvoluted into three peaks. The highest energy peak is assigned to –O–group while the peak at the lowest energy is attributed to –O–C═O group. The peak at ca. 532.6 is assigned to –C–O. It should be noted that the amount of different oxygen functional groups is different for the samples prepared at different the C_{60}/S ratio. This abnormal trend is attributed to the incomplete polymerisation of the sucrose and fullerene molecules in the nanochannels of the KIT-6 template.

The effect of the addition of sucrose molecules in the synthesis mixture affecting the mesostructural order and the morphology of the final MC_{60}@C-X-K hybrids was analysed by high resolution scanning electron microscope and the high-resolution transmission electron microscopy. Figures 5(A)–(D) displayed the HRSEM images of MC_{60}@C-X-K hybrids. It can be seen that the morphology of the template was retained for MC_{60}@C-2-K, MC_{60}@C-1.33-K, and MC_{60}@C-1-K, revealing that the templating process is successful. However, a small degree of distorted

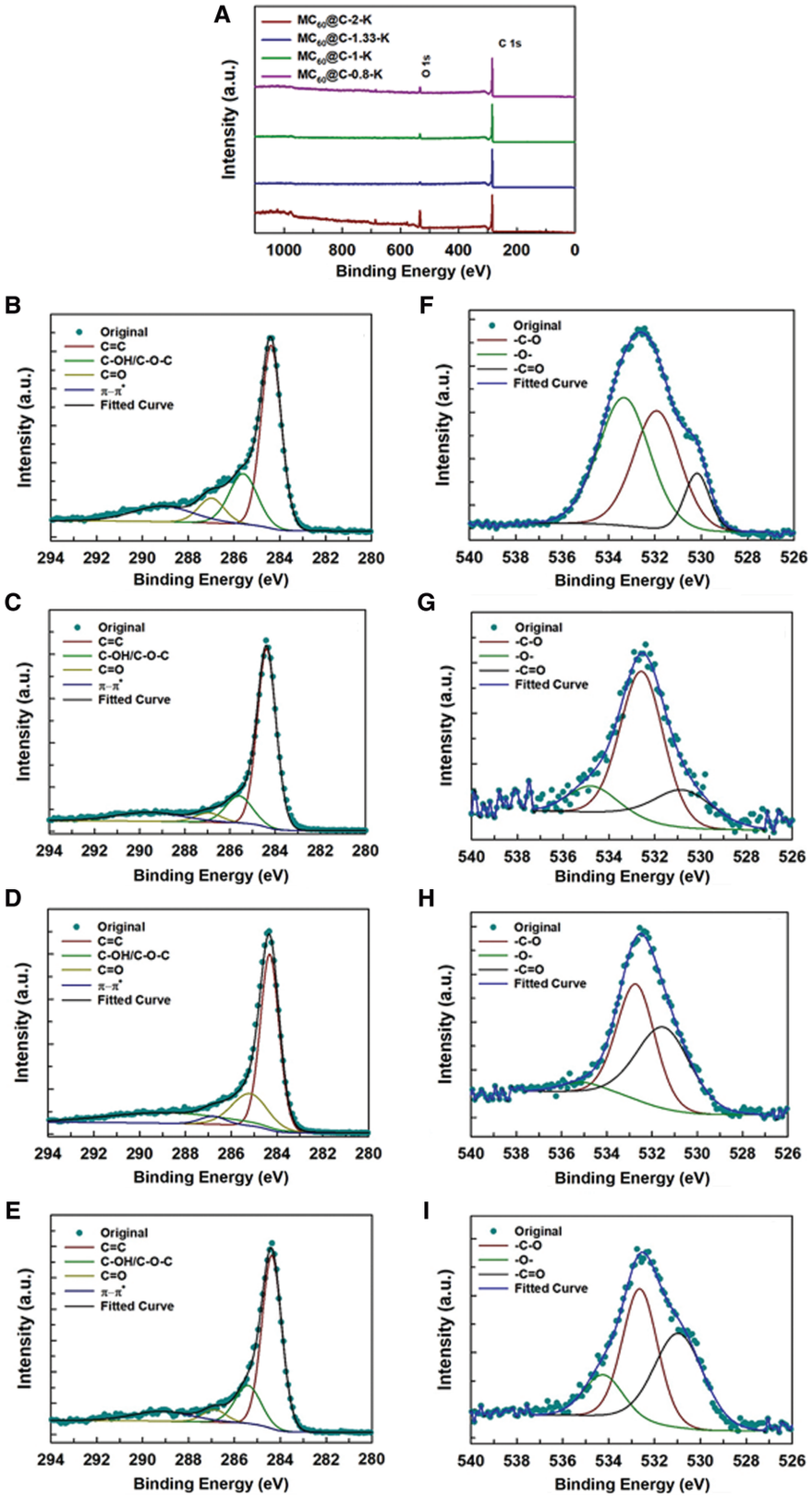

Figure 4. (A) XPS survey, (B–E) C1*s* and (F–I) O1*s* spectra of MC_{60}@C-2-K, MC_{60}@C-1.33-K, MC_{60}@C-1-K, and MC_{60}@C-0.8-K, respectively.

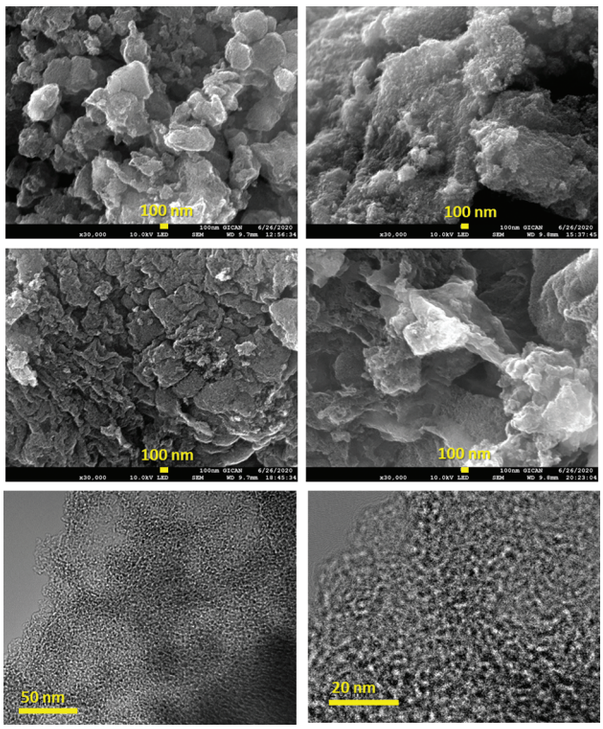

Figure 5. HRSEM images of (A) MC_{60}@C-2-K, (B) MC_{60}@C-1.33-K, (C) MC_{60}@C-1-K, and (D) MC_{60}@C-0.8-K and (E, F) HRTEM images of MC_{60}@C-1-K.

morphology was observed for MC_{60}@C-0.8, suggesting that the replication process was affected by the addition of a large amount of sucrose molecules in the synthesis mixture. To check the ordered and 3D mesoporosity in the sample, we have measured the HRTEM for the representative sample, MC_{60}@C-1-K (Figs. 5(E–F)), which showed well-ordered and 3D mesopores that are crosslinked. This similar structure was also observed for the KIT-6 template, suggesting that the structure of the template was replicated into the MC_{60}@C-1-K.

The favourable textural properties such as high surface area, high conductivity large pore volume, large pore diameter and well-ordered structure of the hybrid material encouraged us to focus on the lithium-ion battery and supercapacitor application. We used three-electrode system to study the performance of cyclic voltammetry and galvanometric charge-discharge of the supercapacitor. Since our material is carbon-based, we selected aqueous 3 M KOH as a suitable electrolyte medium while investigating the potential window from −0.8 to 0.0 V (vs. Ag/AgCl). To fabricate the working electrode, the preparation of a slurry is essential which is formed by grinding the mixture of 5 mg of the composite material with 0.5 mg of acetylene black carbon and polyvinylindene fluoride (PVDF). This slurry was then hard-pressed to nickel mesh which was used as the current collector for the working electrode. The CV of the prepared hybrids measured at a scan rate of 50 mV/S and fixing the potential window from −0.8 to 0 V is shown in Figure 6(A). Typically, EDLC based materials show a quasi-rectangular shape, which is clearly reflected in our mesoporous carbon/C_{60} hybrid as well. As can be seen in Figure 6(A), the specific current increases as the ratio of C_{60}/S is decreased from 2 to 1 and then decreases while the ratio is further reduced to 0.8. The area of CV curve for the MC_{60}@C-1 is the largest which is in good agreement with the specific surface area of MC_{60}@C-1 being highest among all samples. Typically, the carbon-based materials show triangular-shaped charge-discharge, which is again portrayed in all our samples (Fig. 6(B)). Similar to the CV results, the MC_{60}@C-1-K exhibited the highest specific capacitance. With relevance to the best performance of the MC_{60}@C-1, we fully investigated the electrochemical performance of MC_{60}@C-1-K. Figure 6(C) shows the CV curves of MC_{60}@C-1 measured at sweep rates ranging from 5 to 100 mV/s. The sample showed a quasi rectangular-shaped graph for the different scan rates (5–100 mV/s). Through this, the EDLC nature of the sample is confirmed with high stability as well. It should be noted that no reversible redox was noticed in all the CV curves measured at different scan rates. These results confirmed fast-ion transport with the least resistance in the sample, suggesting its suitability for the supercapacitor devices.

To further study the electrochemical behaviour of MC_{60}@C-1-K, the galvanostatic charge-discharge (GCD) measurements at different current densities (0.1–2 A/g) was measured (Fig. 6(D)). The GCD curves of MC_{60}@C-1-K measured at different current densities showed the triangular shape and are almost linear and symmetrical, revealing its robustness and outstanding electrochemical reversibility. The GCD curves showed a steady increase in the specific capacitance from 191 F/g to 254 F/g as the current density was decreased from 2 A/g to 0.5 A/g as shown in Figure 6(D). This value is 1.8 times higher than the pure mesoporous fullerene which can be attributed to the higher surface area, 3D mesoporous structure, better connectivity of C_{60} molecules, and high conductivity due to the carbon layers that connect the fullerene molecules. The low specific capacitance at higher current density may be linked with the electrolyte resistance as it has to travel deep inside the pores and access the active sites. However, the higher specific capacitance of the materials is due to the fact that thin carbon layers offer better stability to the sample by stacking between the fullerene molecules with high order, high conductivity, high surface area and better electronic transport. The specific capacitance of the MC_{60}@C-1-K calculated at the current density of 2 A/g was compared with other porous carbon materials including activated carbon, multiwalled carbon nanotube, mesoporous carbon and mesoporous C_{60} (Fig. 6(E)) [39]. Noteworthy, MC_{60}@C-1-K registered much higher specific capacitance than that of other samples, confirming its

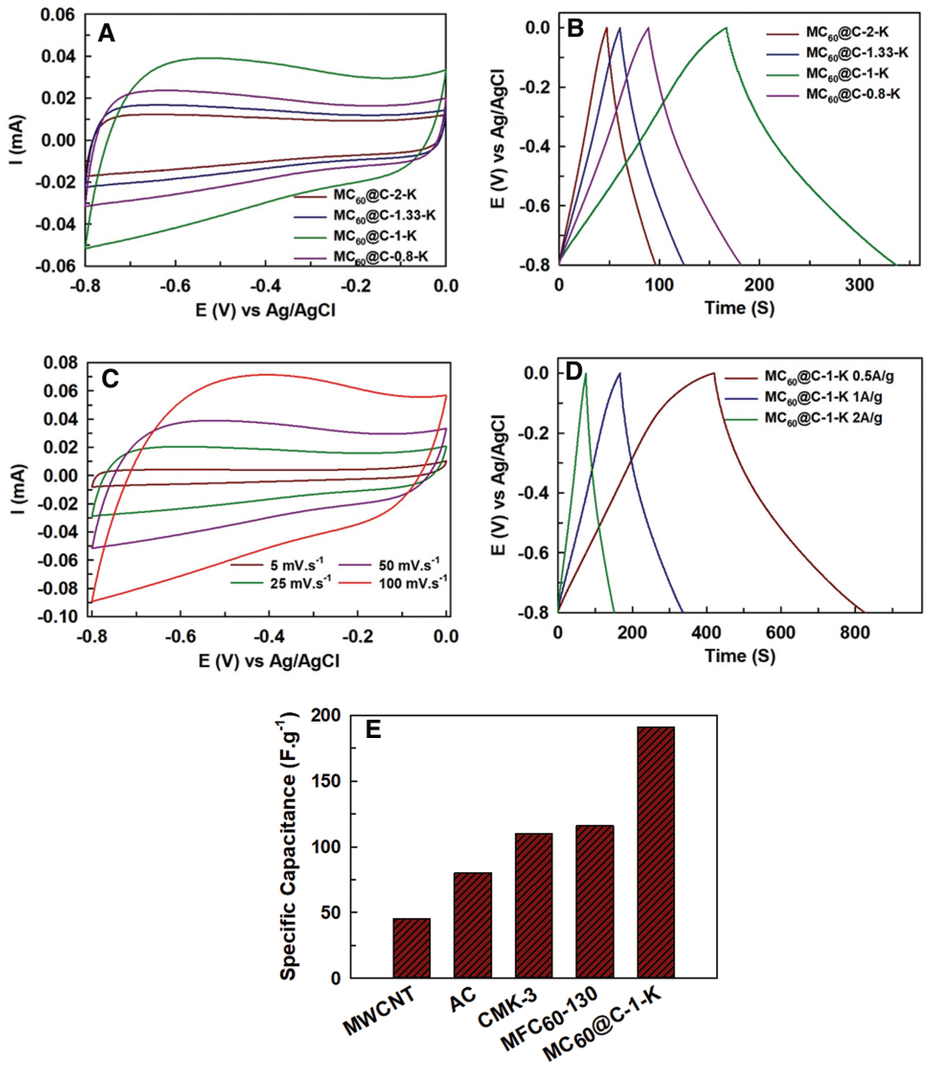

Figure 6. (A) CV of MC_{60}@C-X-K hybrids, (B) gravimetric charge–discharge profiles of MC_{60}@C-X-K measured at 1 A/g, (C) CV curves of MC_{60}@C-1-K at different scan rates from 5–100 mV/s in the potential window between −0.8 to 0.0 V, (D) GCD curves of MC_{60}@C-1-K measured at different current densities from 0.5–2 A/g and (E) comparison of the supercapacitance values of MC_{60}@C-1-K with other samples measured at the current density of 2 A/g.

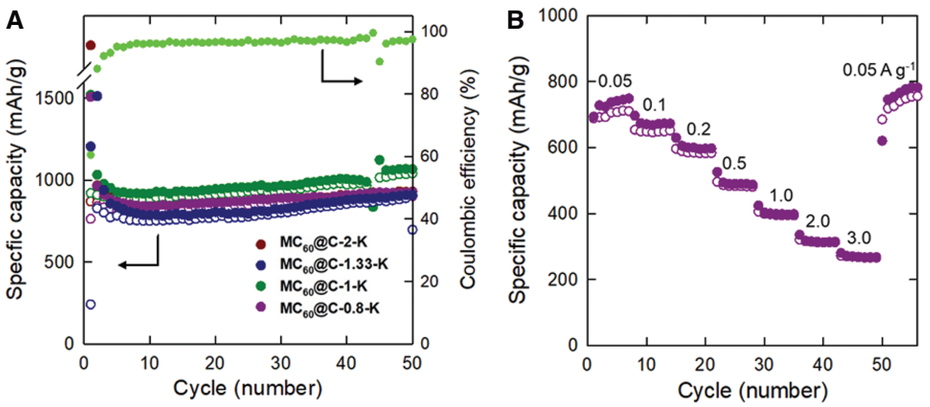

Figure 7. (A) Cycling behaviour of MC_{60}@C-X-K samples in alteration of the ratio of C_{60}/S under a current density of 0.1 A/g. Axis on the right side indicates the Coulombic efficiency of MC_{60}@C-1-K sample during battery cycling. (B) Rate capability performance of MC_{60}@C-0.8-K sample.

superior performance for supercapacitor applications. This high performance of supercapacitor for MC_{60}@C-1-K with high stability is attributed to its three dimensional mesoporous structure, better connection between the fullerene molecules with the thin carbon layers and the surface-active oxygen functional groups which support good diffusion of the electrolyte, ionic conductivity and the charge transfer. The electrochemical stability of the materials was also tested using GCD measurements at the current density of 2 A/g. The sample showed excellent stability even after 100 cycles, indicating the best electrochemical stability for the energy storage devices.

The electrochemical measurement for lithium-ion battery (LIB) performance was carried out under the potential range of 3.0–0.01 V and current density of 0.1 A/g. Among the present samples with varying the ratio of C_{60}/sucrose, the MC_{60}@C-1-K appears to be the most active toward the Li accommodation, which delivers the largest specific capacity of 1067 mAh/g upon 50 cycles (Fig. 7(A)). Further increase of the sucrose amount leads to the slight degradation of specific capacity, showing the specific capacity of 927 mAh/g for MC_{60}@C-0.8-K after 50 cycles. Since the textual property of the sample is closely linked to their capacity behaviour, it is not surprising to see the best battery performance for MC_{60}@C-1-K that possesses the highest specific surface area and porosity [40–41]. It is well-known that the large surface area and porosity would be beneficial in improving battery performance, offering a number of active sites for Li^+ ion accommodation [42]. Relatively low initial Coulombic efficiency (CE) is observed to be ~60% for MC_{60}@C-1-X sample, which is due to the surface electrolyte interface (SEI) formation as a result of chemical reaction with electrolyte. After several cycles, however, it is quickly reached up to over 98%, suggesting stable reversible lithiation-delithiation reaction. Regardless of the ratio of C_{60}/sucrose, all the MC_{60}@C-X-K samples display a quite stable cycling behaviour without any capacity fading. The observed high discharge capacity and stable cycling behaviour could be ascribed to the synergistic effect of the carbon layer and highly ordered mesoporous structure. The carbon layer surrounding the C_{60} molecule could stabilise the SEI layer without further irreversible reaction with electrolyte. Furthermore, by introducing the highly ordered mesoporous structure, specific lithium transport pathway could be established through regular and interconnected pores, significantly shortening the lithium diffusion length. According to the rate capability test of Figure 7(B), quite high specific capacities are observed with different current densities, delivering 737, 668, 600, 489, 403, 315 and 268 mAh/g under current density of 0.05, 0.1, 0.2, 0.5, 1.0, 2.0 and 3.0 A/g, respectively. The promising rate capability could be attributed to the enhanced charge transfer kinetics via wrapping the C_{60} molecule with thin carbon layers. The capacity is fully recovered with returning to the first current density of 0.05 A/g, suggesting the high structural stability and high reversibility during electrochemical cycling.

4. CONCLUSIONS

In summary, we successfully demonstrated the preparation of mesoporous fullerene/carbon hybrids with 3D mesoporous structure through direct synthesis approach via nanotemplating strategy wherein mesoporous silica with 3D mesoporous structure, KIT-6 was used the template. The addition of sucrose molecules not only forms a thin layer between the fullerene molecules but also results in higher specific surface area and pore volume. The prepared hybrid materials exhibited 3D ordered mesoporous structure and have the advantage of fullerene and carbon framework, which can offer the best platform with more electrochemically active sites and electronic conductivity for energy storage applications. The optimised hybrid material showed much higher specific capacitance than other mesoporous fullerenes and porous carbon-based materials. The same material was used as an electrode for Li-ion battery and exhibited a high specific capacity and stability. We surmised that the integration of polymerised fullerenes coupled with the ordered 3D mesoporous carbon wall structure, high specific surface area, specific pore volume and high electronic conductivity facilitates the better electron and electrolyte transport which is key for improving the electrochemical performance. We strongly believe that this simple strategy could be adopted for the fabrication of series of hybrid nanostructures composed of fullerenes and other bio or metal or metal oxide nanostructures which could offer a new platform and expand the application possibilities to adsorption and catalysis.

Conflicts of Interest

There are no conflicts to declare.

Acknowledgments: One of the authors A. Vinu thanks the University of Newcastle for the start-up grant and the Australian Research Council for the award of Discovery Grants (DP170104478 and DP150104828).

References and Notes

1. Azadmanjiri, J., Srivastava, V.K., Kumar, P., Nikzad, M., Wang, J. and Yu, A.M., **2018**. Two- and three-dimensional graphene-based hybrid composites for advanced energy storage and conversion devices. *Journal of Materials Chemistry A*, *6*(3), pp.702–734.
2. Bi, S., Lu, C.B., Zhang, W.B., Qiu, F. and Zhang, F., **2018**. Two-dimensional polymer-based nanosheets for electrochemical energy storage and conversion. *Journal of Energy Chemistry*, *27*(1), pp.99–116.
3. Chen, Q., Tan, X.F., Liu, Y.G., Liu, S.B., Li, M.F., Gu, Y.L., Zhang, P., Ye, S.J., Yang, Z.Z. and Yang, Y.Y., **2020**. Biomass-derived porous graphitic carbon materials for energy and environmental applications. *Journal of Materials Chemistry A*, *8*(12), pp.5773–5811.

4. Chen, C., Tao, L., Du, S.Q., Chen, W., Wang, Y.Y., Zou, Y.Q. and Wang, S.Y., **2020**. Advanced exfoliation strategies for layered double hydroxides and applications in energy conversion and storage. *Advanced Functional Materials*, *30*(14), p.1909832.
5. Schütter, C., Pohlmann, S. and Balducci, A., **2019**. Industrial requirements of materials for electrical double layer capacitors: Impact on current and future applications. *Advanced Energy Materials*, *9*(25), p.1900334.
6. Wu, F.X., Maier, J. and Yu, Y., **2020**. Guidelines and trends for next-generation rechargeable lithium and lithium-ion batteries. *Chemical Society Reviews, 49*(5), pp.1569–1614.
7. Kong, W., Kum, H., Bae, S.H., Shim, J., Kim, H., Kong, L.P., Meng, Y., Wang, K.J., Kim, C. and Kim, J., **2019**. Path towards graphene commercialization from lab to market. *Nature Nanotechnology*, *14*(10), pp.927–938.
8. Cano, Z.P., Banham, D., Ye, S.Y., Hintennach, A., Lu, J., Fowler, M. and Chen, Z.W., **2018**. Batteries and fuel cells for emerging electric vehicle markets. *Nature Energy*, *3*(4), pp.279–289.
9. Benzigar, M.R., Talapaneni, S.N., Joseph, S., Ramadass, K., Singh, G., Scaranto, J., Ravon, U., Al-Bahily, K. and Vinu, A., **2018**. Recent advances in functionalized micro and mesoporous carbon materials: synthesis and applications. *Chemical Society Reviews*, *47*(8), pp.2680–2721.
10. Lakhi, K.S., Park, D.H., Al-Bahily, K., Cha, W., Viswanathan, B., Choy, J.H. and Vinu, A., **2017**. Mesoporous carbon nitrides: Synthesis, functionalization, and applications. *Chemical Society Reviews, 46*(1), pp.72–101.
11. Liu, L.L., Niu, Z.Q. and Chen, J., **2016**. Unconventional supercapacitors from nanocarbon-based electrode materials to device configurations. *Chemical Society Reviews*, *45*(15), pp.4340–4363.
12. Fan, W.J., Zhang, H., Wang, H.L., Zhao, X.C., Sun, S.J., Shi, J., Huang, M.H., Liu, W., Zheng, Y.L. and Li, P., **2019**. Dual-doped hierarchical porous carbon derived from biomass for advanced supercapacitors and lithium ion batteries. *RSC Advances*, *9*(56), pp.32382–32394.
13. Park, J.H., Choi, W.Y., Lee, S., Kim, T.S. and Lee, J.W., **2020**. Graphene intercalated free-standing carbon paper coated with MnO_2 for anode materials of lithium ion batteries. *Electrochimica Acta*, *348*, p.136310.
14. Luo, J.D., Zhang, H., Zhang, Z., Yu, J. and Yang, Z.Y., **2019**. In-built template synthesis of hierarchical porous carbon microcubes from biomass toward electrochemical energy storage. *Carbon*, *155*, pp.1–8.
15. Asim, S., Javed, M.S., Hussain, S., Rana, M., Iram, F., Lv, D., Hashim, M., Saleem, M., Khalid, M., Jawaria, R., Ullah, Z. and Gull, N., **2019**. RuO_2 nanorods decorated CNTs grown carbon cloth as a free standing electrode for supercapacitor and lithium ion batteries. *Electrochimica Acta*, *326*, p.135009.
16. Zhang, Y.Y., Xu, M.S., Wang, Y., Lin, S.S., Ji, L.L., Li, X., Zhang, Y.J. and Zhao, J.B., **2020**. Spray drying-assisted preparation FeSx/C/CNT composite for energy storage and conversion performance. *Journal of Alloys and Compounds*, *834*, p.154916.
17. Shi, X.Z., Zhang, S., Chen, X.C., Tang, T. and Mijowska, E., **2020**. Three dimensional graphene/carbonized metal-organic frameworks based high-performance supercapacitor. *Carbon*, *157*, pp.55–63.
18. Liang, Y.R., Xiong, X., Xu, Z.J., Xia, Q.B., Wan, L.Y., Liu, R.T., Chen, G.X. and Chou, S.L., **2020**. Ultrathin 2D mesoporous TiO_2/rGO heterostructure for high-performance lithium storage. *Small, 16*(26), p.2000030.
19. Ciszewski, M., Szatkowska, E., Koszorek, A. and Majka, M., **2017**. Carbon aerogels modified with graphene oxide, graphene and CNT as symmetric supercapacitor electrodes. *Journal of Materials Science: Materials in Electronics*, *28*(6), pp.4897–4903.
20. Li, X., Tang, Y., Song, J.H., Yang, W., Wang, M.S., Zhu, C.Z., Zhao, W.G., Zheng, J.M. and Lin, Y.H., **2018**. Self-supporting activated carbon/carbon nanotube/reduced graphene oxide flexible electrode for high performance supercapacitor. *Carbon*, *129*, pp.236–244.
21. Li, Z.J., Yang, B.C., Su, Y.L., Wang, H.Y. and Groeper, J., **2016**. Ultrafast growth of carbon nanotubes on graphene for capacitive energy storage. *Nanotechnology*, *27*(2), p.025401.
22. Chen, S., Yeoh, W., Liu, Q. and Wang, G., **2012**. Chemical-free synthesis of graphene–carbon nanotube hybrid materials for reversible lithium storage in lithium-ion batteries. *Carbon*, *50*(12), pp.4557–4565.
23. Mandal, S., Lee, M., Hill, J., Vinu, A. and Ariga, K., **2010**. Recent developments in supramolecular approach for nanocomposites. *Journal of Nanoscience and Nanotechnology, 10*(1), pp.21–33.
24. Niu, Z., Zhang, Y., Zhang, Y., Lu, X. and Liu, J., **2020**. Enhanced electrochemical performance of three-dimensional graphene/carbon nanotube composite for supercapacitor application. *Journal of Alloys and Compounds*, *820*, p.153114.
25. Zhong, C., Wang, J.-Z., Wexler, D. and Liu, H.-K., **2014**. Microwave autoclave synthesized multi-layer graphene/single-walled carbon nanotube composites for free-standing lithium-ion battery anodes. *Carbon*, *66*, pp.637–645.
26. Bairi, P., Shrestha, R.G., Hill, J.P., Nishimura, T., Ariga, K. and Shrestha, L.K., **2016**. Mesoporous graphitic carbon microtubes derived from fullerene C_{70} tubes as a high performance electrode material for advanced supercapacitors. *Journal of Materials Chemistry A*, *4*(36), pp.13899–13906.
27. Gradzka, E., Winkler, K., Borowska, M., Plonska-Brzezinska, M.E. and Echegoyen, L., **2013**. Comparison of the electrochemical properties of thin films of MWCNTs/C60-Pd, SWCNTs/C60-Pd and ox-CNOs/C60-Pd. *Electrochimica Acta*, *96*, pp.274–284.
28. Hetfleisch, F., Gunnarsson, O., Srama, R., Han, J.E., Stepper, M., Roeser, H.P., Bohr, A., Lopez, J.S., Mashmool, M. and Roth, S., **2018**. Chemical effects of alkali atoms on critical temperature in superconducting alkali-doped fullerides. *Physica C: Superconductivity and its Applications*, *546*, pp.34–43.
29. Ramirez, A.P., **2015**. Superconductivity in alkali-doped C_{60}. *Physica C: Superconductivity and its Applications*, *514*, pp.166–172.
30. Takeya, H., Konno, T., Hirata, C., Wakahara, T., Miyazawa, K., Yamaguchi, T., Tanaka, M. and Takano, Y., **2016**. Superconductivity in alkali-doped fullerene nanowhiskers. *Journal of Physics: Condensed Matter*, *28*(35), p.354003.
31. Tang, Q., Ji, Q., Bairi, P., Shrestha, R.G., Hill, J.P., Ariga, K., Shrestha, L.K., Ariga, K., Zeng, H. and Ji, Q., **2017**. Quasi 2D mesoporous carbon microbelts derived from fullerene crystals as an electrode material for electrochemical supercapacitors. *ACS Applied Materials & Interfaces*, *9*(51), pp.44458–44465.
32. Wang, C., Zhang, Y., He, W., Zhang, X., Yang, G., Wang, Z., Ren, M. and Wang, L., **2018**. Na-doped C_{70} fullerene/N-doped graphene/Fe-based quantum dot nanocomposites for sodium-ion batteries with ultrahigh coulombic efficiency. *ChemElectroChem*, *5*(1), pp.129–136.
33. Teprovich, J.A., Weeks, J.A., Ward, P.A., Tinkey, S.C., Huang, C.X., Zhou, J., Zidan, R. and Jena, P., **2019**. Hydrogenated C-60 as high-capacity stable anode materials for Li ion batteries. *ACS Applied Energy Materials*, *2*(9), pp.6453–6460.
34. Benzigar, M.R., Joseph, S., Ilbeygi, H., Park, D.-H., Sarkar, S., Chandra, G., Umapathy, S., Srinivasan, S., Talapaneni, S.N. and Vinu, A., **2018**. Highly crystalline mesoporous C_{60} with ordered pores: A class of nanomaterials for energy applications. *Angewandte Chemie International Edition*, *57*(2), pp.569–573.
35. Benzigar, M.R., Joseph, S., Baskar, A.V., Park, D.-H., Chandra, G., Umapathy, S., Talapaneni, S.N. and Vinu, A., **2018**. Ordered mesoporous C_{70} with highly crystalline pore walls for energy applications. *Advanced Functional Materials*, *28*(35), p.1803701.
36. Benzigar, M.R., Joseph, S., Saianand, G., Gopalan, A.I., Sarkar, S., Srinivasan, S., Park, D.H., Kim, S., Talapaneni, S.N., Ramadass, K. and Vinu, A., **2019**. Highly ordered iron oxide-mesoporous fullerene nanocomposites for oxygen reduction reaction and supercapacitor applications. *Microporous and Mesoporous Materials*, *285*, pp.21–31.

37. Saianand, G., Gopalan, A.-I., Lee, J.-C., Sathish, C.I., Gopalakrishnan, K., Unni, G.E., Shanbhag, D., Dasireddy, V.D.B.C., Yi, J., Xi, S., Al-Muhtaseb, A.H. and Vinu, A., **2020**. Mixed copper/copper-oxide anchored mesoporous fullerene nanohybrids as superior electrocatalysts toward oxygen reduction reaction. *Small*, *16*(12), p.1903937.

38. Vinu, A., Gokulakrishnan, N., Balasubramanian, V.V., Alam, S., Kapoor, M.P., Ariga, K. and Mori, T., **2008**. Three-dimensional ultralarge-pore Ia3d mesoporous silica with various pore diameters and their application in biomolecule immobilization. *Chemistry—A European Journal*, *14*(36), pp.11529–11538.

39. Benzigar, M.R., Joseph, S., Ilbeygi, H., Park, D.H., Sarkar, S., Chandra, G., Umapathy, S., Srinivasan, S., Talapaneni, S.N. and Vinu, A., **2018**. Highly crystalline mesoporous C-60 with ordered pores: A class of nanomaterials for energy applications. *Angewandte Chemie-International Edition*, *57*(2), pp.569–573.

40. Placke, T., Siozios, V., Schmitz, R., Lux, S.F., Bieker, P., Colle, C., Meyer, H.W., Passerini, S. and Winter, M., **2012**. Influence of graphite surface modifications on the ratio of basal plane to "non-basal plane" surface area and on the anode performance in lithium ion batteries. *Journal of Power Sources*, *200*, pp.83–91.

41. Niu, J., Shao, R., Liang, J., Dou, M., Li, Z., Huang, Y. and Wang, F., **2017**. Biomass-derived mesopore-dominant porous carbons with large specific surface area and high defect density as high performance electrode materials for Li-ion batteries and supercapacitors. *Nano Energy*, *36*, pp.322–330.

42. Zhang, S., Zheng, M., Lin, Z., Li, N., Liu, Y., Zhao, B., Pang, H., Cao, J., He, P. and Shi, Y., **2014**. Activated carbon with ultrahigh specific surface area synthesized from natural plant material for lithium-sulfur batteries. *Journal of Materials Chemistry A, 2*(38), pp.15889–15896.

Received: 10 August 2020. Accepted: 31 August 2020.